

# Power contours: optimising sample size and precision in experimental psychology and human neuroscience

Daniel H. Baker<sup>1,2,5</sup>, Greta Vilidaite<sup>1</sup>, Freya A. Lygo<sup>1</sup>, Anika K. Smith<sup>1</sup>, Tessa R. Flack<sup>3</sup>, André D. Gouws<sup>4</sup> & Timothy J. Andrews<sup>1</sup>

1. Department of Psychology, University of York, Heslington, York, YO10 5DD, UK

2. York Biomedical Research Institute, University of York, Heslington, York, YO10 5DD, UK

3. School of Psychology, University of Lincoln, Brayford Pool, Lincoln, LN6 7TS, UK

4. York Neuroimaging Centre, The Biocentre, York Science Park, Heslington, York, YO10 5NY, UK

5. Corresponding author, email: [daniel.baker@york.ac.uk](mailto:daniel.baker@york.ac.uk)

When designing experimental studies with human participants, experimenters must decide how many trials each participant will complete, as well as how many participants to test. Most discussion of statistical power (the ability of a study design to detect an effect) has focussed on sample size, and assumed sufficient trials. Here we explore the influence of both factors on statistical power, represented as a two-dimensional plot on which iso-power contours can be visualised. We demonstrate the conditions under which the number of trials is particularly important, i.e. when the within-participant variance is large relative to the between-participants variance. We then derive power contour plots using existing data sets for eight experimental paradigms and methodologies (including reaction times, sensory thresholds, fMRI, MEG, and EEG), and provide estimates of the within- and between-participant variance for each method. In all cases, the within-participant variance was larger than the between-participants variance, meaning that the number of trials has a meaningful influence on statistical power in commonly used paradigms. An online tool is provided (<https://shiny.york.ac.uk/powercontours/>) for generating power contours, from which the optimal combination of trials and participants can be calculated when designing future studies.

**Keywords:** statistical power, sample size, neuroscience, psychophysics, fMRI, MEG, EEG

## Introduction

Statistical power is the ability of a study design with a given sample size to detect an effect of a particular magnitude. In recent years, the problems with low statistical power have been increasingly highlighted. Low powered studies are less able to detect a true effect (and so make Type II errors), and are therefore more likely to report spurious effects (Type I errors) compared with high-powered studies. Furthermore, any real effects that are detected are likely to have inflated effect sizes (Colquhoun, 2014; Ioannidis, 2008). These problems are common across many scientific disciplines, and estimates of power across studies in the neurosciences (Button et al., 2013) yield power values in the range 8%-30%, far below the desired level of  $\geq 80\%$ . The prevalence of low-powered studies has filled some areas of the literature with effects that fail to replicate and may well be spurious (Ioannidis, 2005; Open Science Collaboration, 2015). Most discussion of increasing statistical power has focussed on recruiting larger sample sizes, because for a given effect size, power is a function of sample size (see Figure 1d). However there is a second degree of freedom available to many experimenters at

the study design stage – the number of repetitions (or trials) of a given experimental condition by each participant.

When the dependent variable of interest can be estimated with high precision, repeated measurements provide little benefit, and the main source of variance is between participants. This is illustrated by the distribution in Figure 1a, where participants (points) differ according to a normal distribution (curve), but the variance of each individual point is negligible. A more realistic situation for many experimental paradigms is shown in Figure 1b, where the variance of each individual estimate is large, as indicated by the horizontal standard error bars. This has the knock-on effect of increasing the overall standard deviation of the sample ( $\sigma_s = 2$  units in Figure 1a, and  $\sigma_s = 3$  units in Figure 1b). Such inflation of the sample standard deviation can be ameliorated by improving the accuracy of each participant's estimated mean by increasing the number of measurements. This is demonstrated in Figure 1c, where each participant's mean is estimated from  $k=200$  trials (compared with  $k=20$  in Figure 1b), and the standard deviation of the sample (curve) reduces substantially (to  $\sigma_s = 2.1$  units).

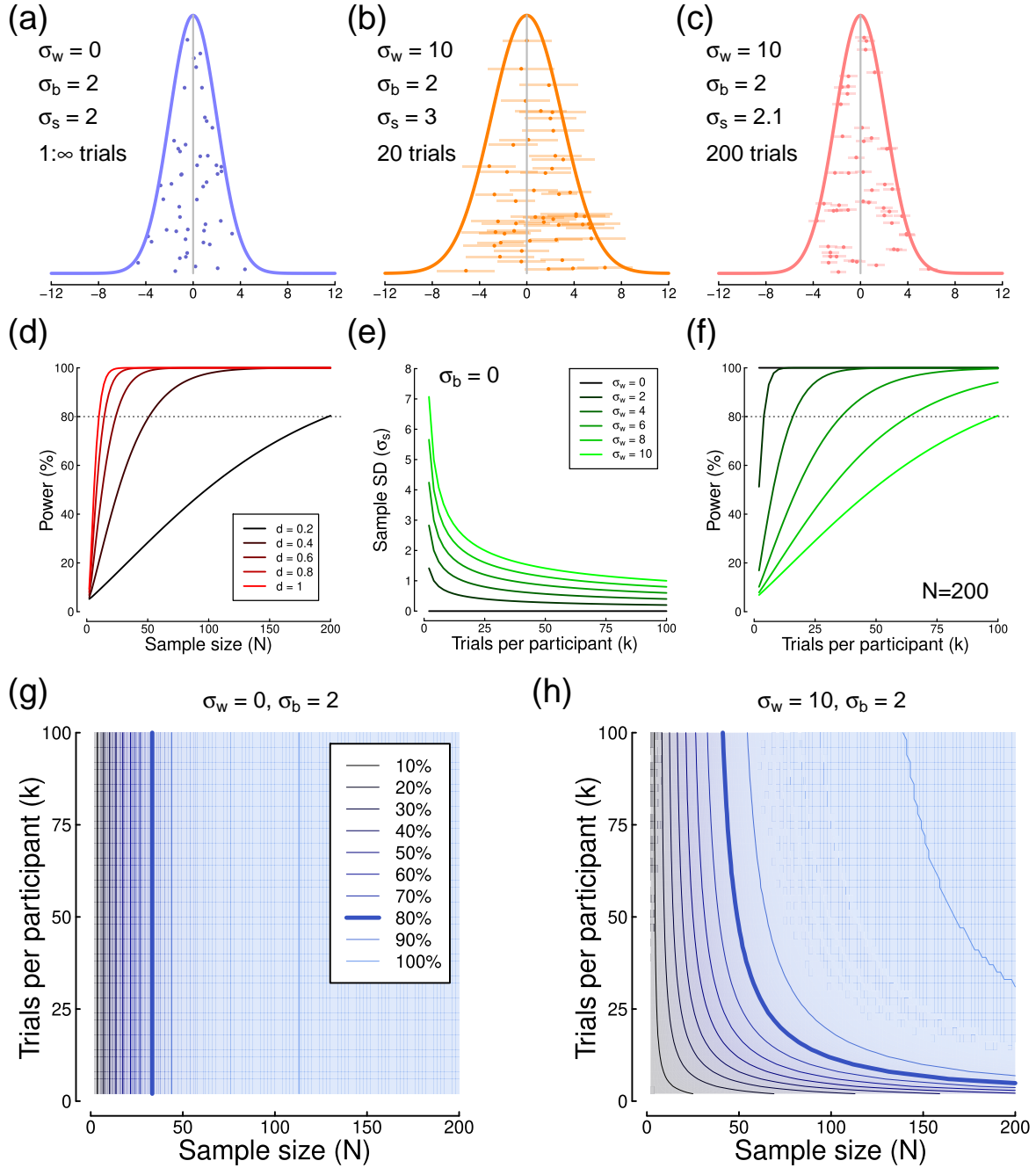


*Figure 1.* Simulations of standard deviation and statistical power. Panel (a) shows simulated data for 50 individuals, generated using a population mean of  $M = 0$ , a within-participants standard deviation of  $\sigma_w = 0$ , and a between-participants standard deviation of  $\sigma_b = 2$ . In panel (b) the within-participant standard deviation was increased to  $\sigma_w = 10$ , and each point is the mean of 20 trials, with horizontal error bars indicating  $\pm 1$  SEM. Panel (c) shows the effect of increasing to 200 trials per participant. Panel (d) plots traditional power curves for different effect sizes (Cohen's  $d$ ) as a function of sample size ( $N$ ). The dashed horizontal line indicates a power of 80%, which is generally considered acceptable. Panel (e) shows how the sample standard deviation ( $\sigma_s$ ) depends on the number of trials per participant ( $k$ ) for a range of within-participant standard deviations (see legend), and a between-participant standard deviation of  $\sigma_b = 0$ . Panel (f) shows the statistical power resulting from the values in panel (e), for a sample size of  $N=200$  and an underlying mean of  $M = 0.2$ . Panels (g,h) show power contours for different combinations of  $\sigma_w$  and  $\sigma_b$ , as described in the text. Simulations used normally distributed random numbers, and statistical power was calculated for a two-sided, one-sample t-test comparing to a mean of 0.

Power is typically derived using effect size measures such as Cohen’s  $d$  (Cohen, 1988), which depends on the sample mean (or difference in means), and also the sample standard deviation (formally  $d = M/\sigma_s$ ). Under parametric assumptions, the number of trials per participant ( $k$ ) influences the sample standard deviation (Figure 1e), according to the equation:

$$\sigma_s = \sqrt{\sigma_b^2 + \frac{\sigma_w^2}{k}} \quad (1)$$

where  $\sigma_b$  and  $\sigma_w$  are the between- and within-participant standard deviations, and  $k$  is the number of trials per participant. The sample standard deviation ( $\sigma_s$ ) determines the effect size, and subsequently the power (Figure 1f). In domains where the dependent variable is subject to high variance (as is typically the case in psychology and neuroscience studies), increasing the precision of the per-participant estimate can therefore greatly increase overall power, perhaps reducing the number of participants required for a study (see Cleary & Linn, 1969; Phillips & Jiang, 2016). Although most active researchers are intuitively aware of this fact (it is common knowledge that running lots of trials delivers “better” data), and the problem has received mathematical treatment (Kanyongo, Brook, Kyei-Blankson, & Gocmen, 2007; Phillips & Jiang, 2016; Rouder & Haaf, 2018; Williams & Zimmerman, 1989), there is no widely used procedure for quantitatively determining the appropriate number of trials to run. Nor are there estimates of typical within- and between-participant variance available that could be incorporated into such calculations for widely-used techniques in experimental psychology and human neuroscience. Instead, studies are typically designed using rules of thumb, prior precedent and guesswork.

In this paper, we advocate a useful representation, the *power contour* plot – a two-dimensional representation of power as the joint function of sample size ( $N$ ) and number of trials ( $k$ ). We provide an online tool for generating power contours in order to estimate the impact of measurement precision (the number of trials conducted) on statistical power. We then use existing data sets to explore the joint effects of sample size and number of trials on real data sets using common methodologies and paradigms in psychology and neuroscience research. These measures include reaction times, psychophysical thresholds, event-related potentials, steady-state evoked potentials, and fMRI BOLD signals. Crucially, our inclusion of empirical data provides an estimate of typical parameter values that could be used in the design of future studies.

## Power contours

Consider first the situation described above, in which the dependent variable of interest can be estimated accurately from a single trial, but individuals all express different true values of the variable (formally, the within-participant variance is low, but the between-participant variance is high,  $\sigma_w \ll \sigma_b$ ). Examples might include variables such as age and height, for which there is low measurement error and minimal variation from moment to moment, or for which tools exist (such as tape measures) to facilitate accurate measurement. In these situations, statistical power is a function of sample size and effect size (Figure 1d), where effect size is Cohen’s  $d$ . Clearly, in such a situation, testing each participant multiple times should confer no advantage. We can represent the power as a function of both sample size and number of trials using a 2D plot such as the one shown in Figure 1g. Here the lines trace iso-power contours – combinations of sample size and number of trials that result in the same statistical power. For this example the power contours are vertical, showing no benefit of repeated testing.

Next consider a more realistic scenario – a situation where the individual measurements are very noisy (high within-participant variance relative to the between-participant variance,  $\sigma_w > \sigma_b$ ). The sample standard deviation decreases as a function of the number of trials (Figure 1e), as the estimated mean for each participant becomes more accurate with repeated measurements. Now power depends on both the number of trials and the sample size, and a series of curved iso-power contours are apparent (Figure 1h).

These power contours offer a useful summary of the effect of possible experimental designs on statistical power. A given power (e.g. 80%, given by the thick blue curves on the power contour plots) can be obtained from multiple combinations of sample size and trial number. This is a useful insight, as study designs can then be optimised depending on other constraints. If relatively few participants are available (perhaps because of financial constraints, or testing of a clinical population) then the number of trials can be increased. Note, however, that beyond a particular number of trials (around  $k=50$  in Figure 1h), the function asymptotes and further trials are not beneficial. Alternatively, if each participant must be tested very rapidly (e.g. for studies involving children), but many participants are available, the number of trials could be kept relatively low (here around  $k=20$ ), and a larger sample size tested. This is of potential value for large cohort studies, in which many participants each complete a large battery of various tasks. A more typical situation is one in which an experimenter wishes to minimise both sample size and testing time – here values around the knee-point of the power contour permit joint optimisation of both parameters. Power contour plots can be produced for any combination of

within- and between-participant variances and difference in means using an *R* script, which can be accessed through a web interface at: <https://shiny.york.ac.uk/powercontours/>

To have practical value in the design of experiments, it is necessary to have some idea of the relative levels of within and between participant variance for the experimental paradigm one intends to use. To this end, we have reanalysed data from 8 studies, using a range of common methodologies from psychology and cognitive neuroscience, including proportional choices, reaction times, sensory thresholds, EEG, MEG and fMRI. We estimate power contours by subsampling the data, so we aimed to include data sets featuring large sample sizes, in which each participant completed many trials (though it was not always possible to satisfy both criteria). All of these analyses are based on one-sample or paired t-tests, but the same principle applies to more sophisticated statistical techniques. All analysis scripts are available on the project repository at <https://osf.io/ebhmk/> and data sets are provided either on the project page or referenced directly throughout the manuscript. We anticipate that these resources are most valuable as a guideline for performing related analyses for specific study designs, and suggest that readers short on time might find it most useful to skip ahead to the section reporting data from whichever paradigm they are most familiar.

### Proportional choices in the Iowa Gambling Task

We reanalysed a data set comprising  $N=504$  participants in the Iowa Gambling Task, as reported by Steingrover et al. (2015), and made publicly available through that publication. In this task, participants choose cards from four decks. Two decks have a greater overall payoff ('good' decks), and the other two have a poorer payoff ('bad' decks). Participants must learn these contingencies during the course of the experiment, and attempt to maximise their payoff. Figure 2a shows summary data for a population of participants who each completed  $k=100$  trials of the task. Averaged across all trials, the mean probability of selecting a 'good' card from a 'good' deck was 0.54 (sample SD of  $\sigma_s = 0.16$ ), an effect size of  $d=0.24$  when compared with the chance baseline of 0.5. The black trace illustrates that at the start of the experiment participants are more likely to choose cards from the 'bad' decks for around the first 20 trials. Their behaviour then changes as they learn the task contingencies, and for the final 40 trials they are more likely to choose cards from the 'good' decks.

We calculated power by resampling random subsets of trials and participants from the data, and calculating the effect size and power using the mean and standard deviation, for a one-sample t-test comparing to 0.5 (using the *pwr.t.test* function in the *pwr* package in *R*). This procedure was repeated

10,000 times, and the averaged power estimates are shown in Figure 2b. As predicted by the simulations in Figure 1h, power depends on both sample size and number of trials. With small numbers of trials ( $k < 40$ ), sample size can be dramatically reduced by increasing trial numbers. For example, by increasing from  $k=5$  to  $k=40$  trials, the sample size can be reduced from  $N=400$  to  $N=200$  whilst maintaining power. Alternatively, for a sample size of  $N=200$ , there are few gains to be made by increasing from  $k=40$  to  $k=100$  trials, as the function has reached asymptote.

In the Iowa Gambling Task, the trial contingencies are learned throughout the experiment, and this information is lost by randomly sampling trials as we did to generate the power contour plot in Figure 2b. An alternative is to retain the trial order, and resample only across participants. Power contours are shown for this analysis in Figure 2c. Over the first 40 trials, power is high because the mean probability is significantly below 0.5 (see black curve in Figure 2a). As participants start to learn the task contingencies, the mean probability passes through 0.5, and power falls to near zero around 60 trials. Then, as participants begin to reliably choose the 'good' deck, the average probability becomes significantly above 0.5 and power increases again, reaching 80% by around 80 trials with the full sample of participants.

Overall, the data from the Iowa task validates the basic predictions from our simulations. The power contours in Figure 2b have the expected shape, and permit joint estimation of the required numbers of trials and participants to achieve appropriate statistical power. We have also shown that a variant of our resampling procedure can provide an alternative visualisation of the data set (Figure 2c), showing how performance changes over time.

### Reaction times

We next analysed reaction time measures from a Posner-style attentional cueing experiment previously reported by Pirrone, Wen, Li, Baker, and Milne (2018). Participants ( $N=38$ ) saw a central cue stimulus directing their attention to either the left or the right of fixation. A sine wave grating target was then presented either in the attended location (congruent condition) or the unattended location (incongruent condition). Each participant completed  $k=600$  congruent trials and  $k=200$  incongruent trials, but we downsampled the congruent data to give equal sample sizes in the two conditions, with example RT distributions for one participant shown in Figure 3a. As is typically observed for reaction time data, the results were positively skewed on linear axes, so we plot them here on logarithmic axes and performed all calculations on log-transformed values. At the group level, reaction times were on average 46 ms slower in the incongruent condition (see Figure 3b), and the standard deviation of

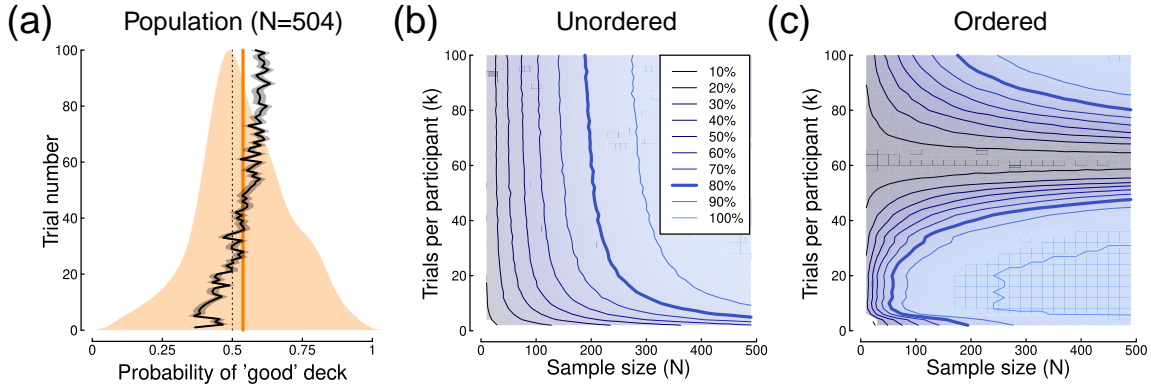


**Figure 2.** Summary of proportion data from the Iowa Gambling task. Panel (a) shows a histogram of the mean probability of choosing a card from a ‘good’ deck for the population of  $N=504$  participants, each averaged across  $k=100$  trials. The vertical orange line shows the grand mean, and the dashed vertical line is the probability expected by chance. The black curve (with grey shading showing  $\pm 1SE$ ) shows the mean probability across all participants on each trial (1 to 100). Panel (b) shows power contours for one-sample t-tests comparing the mean probability to the chance baseline (0.5). For these simulations, trials were randomly subsampled. Panel (c) shows power contours when trials were included sequentially.

the differences was 43 ms. For the full data set, this yielded an effect size of  $d=1.1$ .

The power contour plot for this data set is shown in Figure 3c, and was generated by randomly subsampling the data set for different combinations of sample size and trial number as described above. Just as predicted by our simulations (Figure 1h), the iso-power contour for 80% power (shown by the thick blue line) is curved. High power can be obtained with either a large sample size ( $N>20$ ) and small number of trials ( $k<10$ ) or a large number of trials ( $k>50$ ) and small sample size ( $N=8$ ). The knee-point of the function is around a sample size of  $N=12$ , with each participant completing approximately  $k=20$  trials. Of course, this is for a relatively large effect size with a robust and well-established effect (attentional cueing). Other study designs with smaller sized effects will require larger sample sizes and/or more trials, but it is clear that the same basic pattern should apply for experiments of this type.

### Sensory thresholds

Psychophysical detection thresholds are typically measured using large numbers of binary trials across stimuli of different intensities. The proportion of correct trials increases monotonically with stimulus intensity, producing a psychometric function (see Figure 4a). Threshold is then estimated at some criterion performance level (often 75% correct) by fitting a continuous ogival function such as a cumulative Gaussian or Weibull distribution. We reanalysed

data from a binocular summation experiment (reported by Baker, Lygo, Meese, & Georgeson, 2018), in which contrast detection thresholds were measured in this way for sine wave grating stimuli shown either monocularly or binocularly using a stereo shutter goggle system. Example psychometric functions for a single participant are shown in Figure 4a (fitted using the *quickpsy* package in R, see Linares & López-Moliner, 2016), where it is clear that equivalent performance requires higher contrast for monocular presentation (orange) than for binocular presentation (green). At the group level (see Figure 4b), this produces a ratio of monocular to binocular thresholds between  $\sqrt{2}$  and 2 – the well-known binocular summation effect – which here had an effect size of  $d=1.8$ .

We resampled the data set to produce the power contour plot shown in Figure 4c. Because each participant completed slightly different numbers of trials (owing to the adaptive staircase procedure used to determine contrast levels for each trial), we subsampled at different percentages of trials for each participant. On average, each participant completed 225 trials for the binocular condition, and for the monocular conditions for each eye (left and right eyes were tested separately and their data combined). Summation estimates were rejected when they fell outside of a reasonable range (between factors of 0.12 and 32), as this indicated that something had gone wrong with the fitting procedure. As anticipated, power depended on both sample size and number of trials, and continued to improve over the ranges available in the data set (i.e. the function at 80% power was quite shallow, and did not asymptote over the ranges tested). Indeed, with all trials included, only around six participants were required

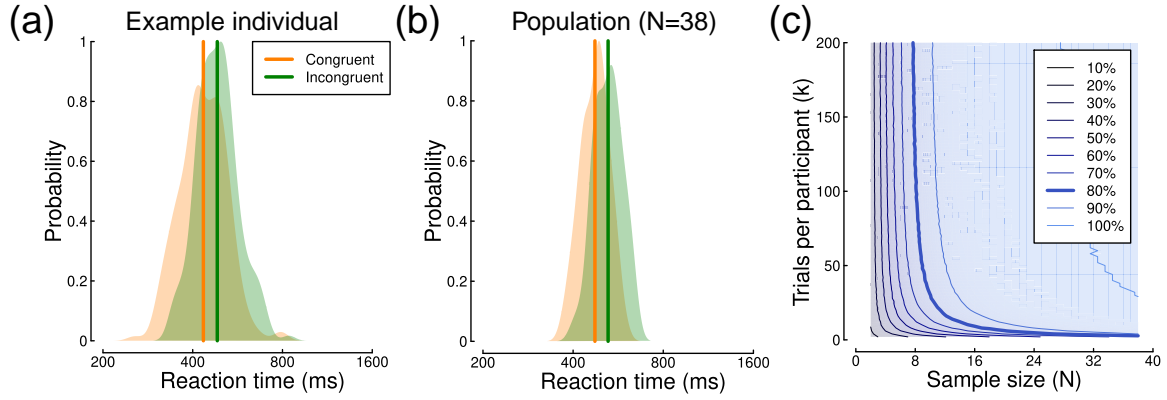


*Figure 3.* Summary of reaction time data. Panel (a) shows reaction time distributions for an example participant, with vertical lines giving the means (of log-transformed values). Panel (b) shows the group level data for mean reaction times across the sample of 38 participants. Panel (c) shows a power contour plot, in which colour represents statistical power (see legend). The thick blue line indicates combinations of sample size and trial number with a power of 80%.

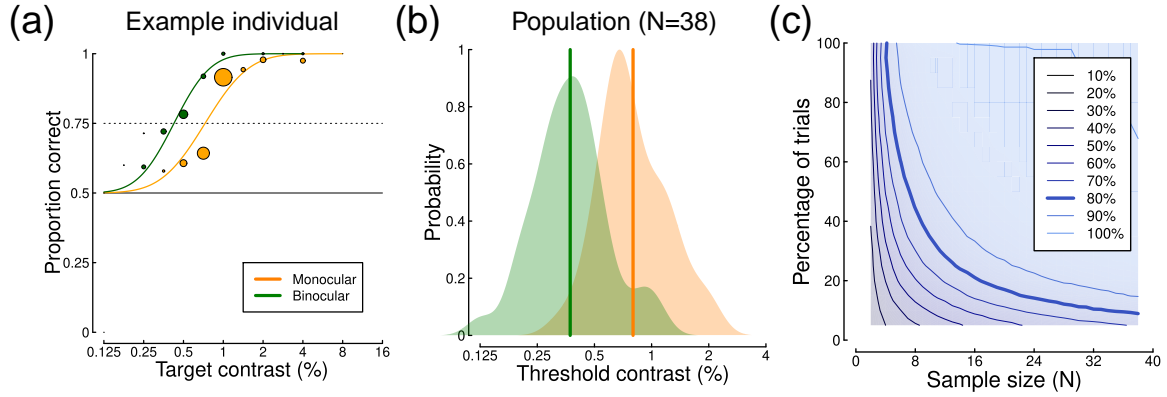


*Figure 4.* Summary of threshold psychophysics data. Panel (a) shows psychometric functions for a single participant, with symbol size proportional to the number of trials at each target contrast level. Curves are fitted cumulative Gaussian functions, used to interpolate thresholds at 75% correct (dashed line). Data for the monocular condition (orange) were pooled across the left and right eye conditions before fitting. Panel (b) shows distributions of monocular (orange) and binocular (green) detection thresholds across a group of  $N=38$  participants with normal vision. Panel (c) shows the power contours derived by subsampling the data and refitting the psychometric functions.

to reach 80% power (consistent with previous estimates of power for this paradigm, see Baker et al., 2018). Conversely, when all 38 participants were included, only around 15% of trials were required (around 34 trials for each condition). Alternatively, 80% power could be maintained with a sample size of  $N=12$  each completing around 30% of the total trials.

### EEG: event-related potentials

We next analysed event-related potentials from a contrast discrimination experiment reported by Vilidaite, Marsh, and Baker (2019), recorded using a 64-channel EEG cap. The stimuli were sine wave gratings with a contrast of 50%, presented for 100 ms. These produced a typical response (see Figure 5a) over occipital electrodes (see Figure 5b), with positive peaks at around 120 and 220 ms (marking stimulus onset and offset), and a later negative region with a trough around

600 *ms*. Each trial was normalised to the voltage during the 200 *ms* before stimulus onset. The sample size for this experiment ( $N=22$ ) was modest (albeit typical for ERP research), but each participant completed a very large number of trials ( $k=1200$ ). We selected three time points (96, 147 and 226 *ms*), with mean voltages of 2, 4 and 8  $\mu\text{V}$  relative to baseline (see coloured markers in Figure 5a), equating to effect sizes (Cohen's  $d$ ) of 0.6, 0.9 and 1.63. Distributions of voltages for an example individual and for the group are shown in Figure 5c,d.

We calculated power contours for each of the three time points, as shown in Figure 5e-g. These have the expected format, though the smallest effect reached only 60% power with the full data set. Across all time points, power reached asymptote at around  $k=300$  trials with negligible further improvements beyond this. Across most of the range of trial numbers, power was largely determined by sample size, and only for relatively few trials ( $k<100$ ) could sample size be materially reduced by adding more trials. This suggests that the major limitation on statistical power in typical ERP experiments (which traditionally involve several hundred trials per condition) is the between-participant variance, rather than the within-participant variance. We will return to this point below.

### EEG: steady-state evoked potentials

An alternative EEG paradigm is the steady-state method, where a stimulus oscillates at a particular frequency, inducing entrained neural responses at that same frequency. In an experiment reported by Vilidaitė et al. (2018), sine wave gratings of different contrasts were flickered at 7Hz, and shown to a sample of  $N=100$  participants. Each participant completed 8 trials of 11 seconds per contrast level, from which the first 1s of EEG data was discarded, and the remaining 10s were divided into 10 epochs of 1s each, yielding a total of  $k=80$  observations per condition. Each epoch was then Fourier transformed, and responses are evident both at the fundamental (flicker) frequency (7Hz) and its second harmonic (14Hz), as shown in Figure 6a. For these visual stimuli, the responses are strongest at the occipital pole, near early visual cortex (see inset to Figure 6a).

Responses at the fundamental frequency increase monotonically with maximum stimulus contrast (see Figure 6b) at electrode  $O_z$ . For a stimulus contrast of 8% (marked by the green point), comparing absolute responses (i.e. removing the phase component before averaging) to the baseline condition (0% contrast, orange point) results in an effect size of  $d=0.2$ . However this can be substantially increased (to  $d=0.68$ ) by using coherent averaging, in which both the amplitude and phase information are averaged across trials for each individual participant (and the absolute amplitudes

are then averaged across participants). The improvement occurs because responses to the stimulus are phase-locked, and therefore should have the same phase on each trial. Any noise at the stimulus frequency has random phase, and so cancels out over multiple repetitions. Example Fourier spectra for both coherent (blue) and incoherent (red) averaging methods are shown in Figure 6a, where it is clear that the coherent method greatly reduces the noise at off-target frequencies. Note in particular the increase in noise in the alpha band (8-12Hz) is clear with incoherent averaging (red) but absent with coherent averaging (blue). In the contrast response function (Figure 6b), coherent averaging (blue function) leads to lower amplitudes at low stimulus contrasts, whereas with incoherent averaging (red function) responses must overcome a much higher 'noise floor' before they can be detected. Distributions of voltages for an example participant and for the population are shown in Figure 6c,d.

We calculated power contours using both coherent (Figure 6e) and incoherent (Figure 6f) averaging, which further confirmed that coherent averaging results in substantially greater statistical power. The 80% power contour in the coherent condition (thick line in Figure 6e) is relatively shallow, showing that both increasing sample size and adding more trials will improve power over most of the range explored here. For example, halving the sample size from  $N=100$  to  $N=50$  requires an increase from approximately  $k=20$  to  $k=40$  trials per participant to maintain power at 80%. We confirmed these general findings at the higher stimulus contrasts (not shown).

### fMRI: event-related design

A widely-used fMRI paradigm is the event-related design, in which stimuli are presented briefly with a jittered inter-stimulus interval (ISI). We obtained data from the Cam-CAN project, conducted by the Cambridge Centre for Ageing and Neuroscience (<http://www.cam-can.org/>) for an event-related fMRI experiment detailed by Shafto et al. (2014) and Taylor et al. (2017). In brief,  $N=645$  participants viewed bilateral checkerboard patterns, presented for 30 *ms* and repeated  $k=124$  times. Some stimuli were accompanied by an auditory beep, but this was disregarded for the purposes of our analyses.

We implemented a minimal preprocessing pipeline using FSL (Jenkinson, Beckmann, Behrens, Woolrich, & Smith, 2012). This involved co-registering the functional data to an individual participant's anatomical scan, and then to the standard MNI152 brain. We used the inverse of these transforms to project a probabilistic map of primary visual cortex (V1) obtained from Wang, Mruczek, Arcaro, and Kastner (2015) onto the functional data to use as a region of interest (see Figure 7a). The functional data were corrected



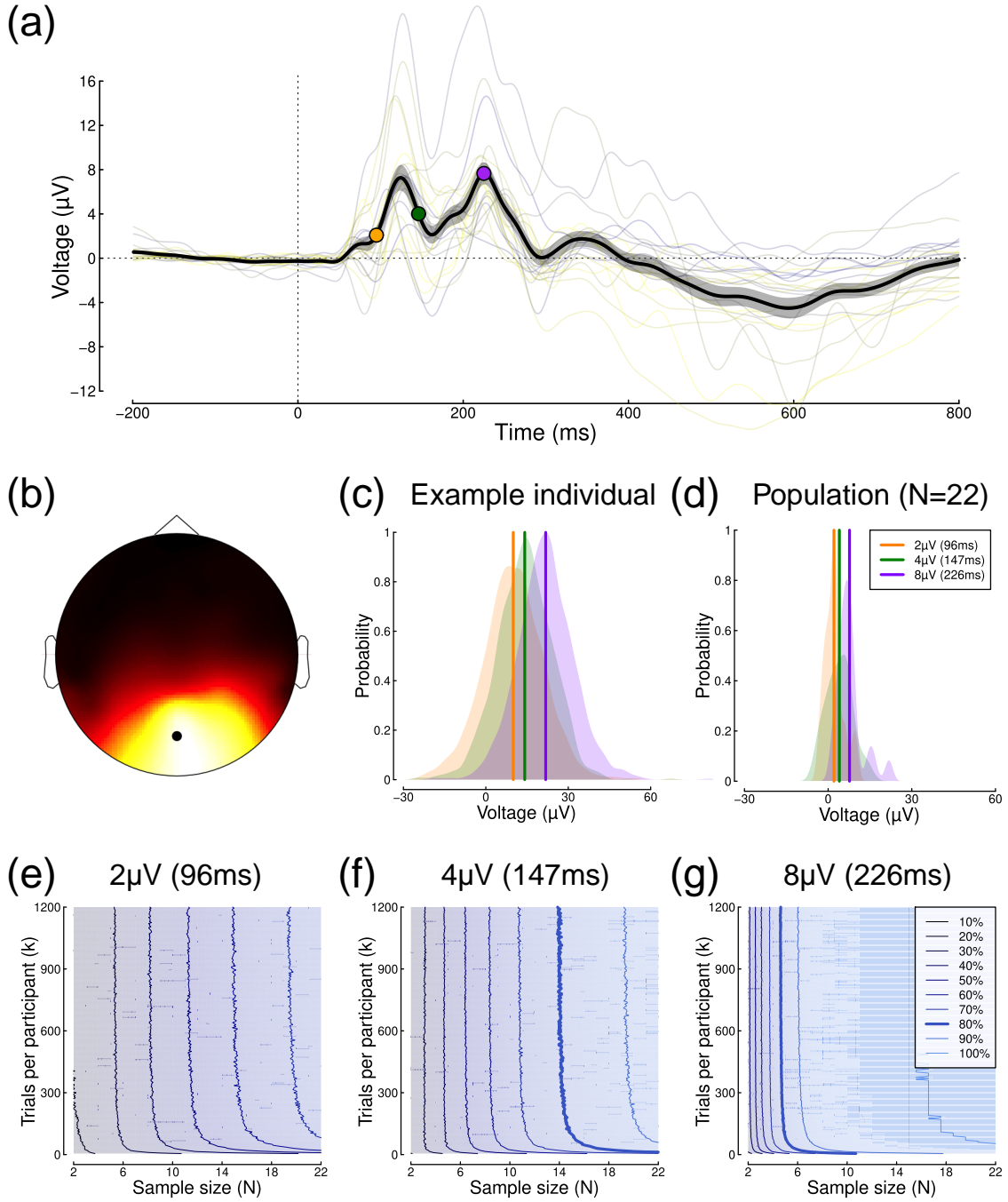


*Figure 5.* Summary of ERP results. Panel (a) shows a grand mean ERP in response to central presentation of a 50% contrast sine wave grating. Thin traces show individual participants ( $N=22$ ), and the grey shaded region shows  $\pm 1\text{SE}$  across participants. Panel (b) shows the distribution of voltages across the scalp at 226 ms after stimulus onset (marked by the purple point in panel a). The black symbol marks electrode  $Oz$ , from which ERPs were taken. Panel (c) shows distributions of voltages across trials at three time points for a single participant. Panel (d) shows average voltages across a group of  $N=22$  participants. Panels (e-g) show power contours at three time points, corresponding to three different average voltages.



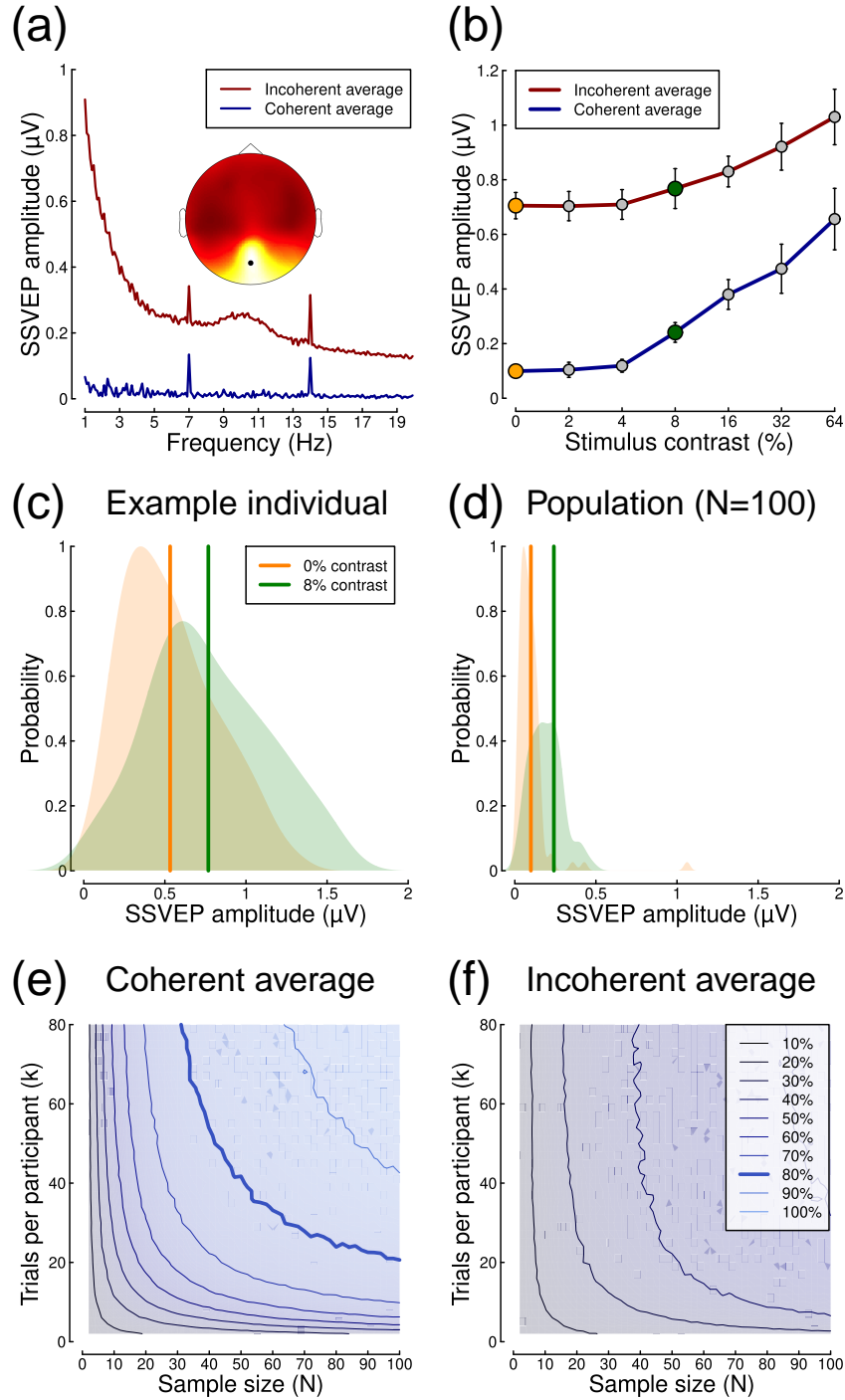


*Figure 6.* Summary of SSVEP data. Panel (a) shows Fourier spectra for full 10 s long trials, using either coherent (blue) or incoherent (red) averaging, and the scalp distribution of activity at 7Hz (inset). Panel (b) shows contrast response functions for both types of averaging. Panel (c) shows the distribution of amplitudes for an example participant, and panel (d) shows averages for the population. Panels (e) and (f) show power contours for coherent and incoherent averaging, respectively.

for slice timing and participant motion, and high pass filtered at 0.01Hz. Then the time-course was averaged across the V1 ROI and exported for further analysis. Whilst this anatomically-defined ROI will necessarily include some voxels that were not responsive to the stimulus, we would expect noise from these voxels to average out and not adversely affect our results (e.g. Boynton, Engel, Glover, & Heeger, 1996).

We then constructed general linear models (GLMs) for each data set using the individual trial timings. To simulate experiments with variable numbers of trials, each GLM split the data using random trial allocations into two arbitrary groups – a ‘target’ condition and a ‘non-target’ condition. A third condition modelled four auditory-only trials which lacked any visual stimulus. A canonical double gamma haemodynamic response function (Figure 7b) was convolved with each condition using the *fmri.stimulus* function (part of the *fmri* package in *R*, see Tabelow & Polzehl, 2011), and orthogonal second order polynomial drift terms were included in the overall model. We then fit the GLM to determine a regression (beta) weight for the target condition to use as our dependent variable. By varying the number of trials allocated to the target and non-target conditions, we were able to simulate experiments with different numbers of trials, whilst keeping the GLM design balanced (see Figure 7c). To provide a null condition, we repeated the analysis using randomly determined events within the experiment time-course (i.e. not using the true event timings). This generated the sample distributions of beta weights shown in Figure 7d, and resulted in an effect size of  $d=0.9$  for the full data set.

We calculated effect sizes across participants for the difference between beta values for the true and null models with different numbers of trials (see Figure 7c), and used these to estimate statistical power. As previously, simulations were repeated 10,000 times with different random sampling of trials and participants to generate power contours (see Figure 7e). As with several previous data sets, power continued to increase across the full range of trial numbers, such that 80% power could be maintained for sample sizes from  $N=20$  to  $N=600$ , simply by varying the number of trials. This flexibility allows event-related designs to achieve high statistical power even with relatively modest sample sizes, but it is critical that sufficient trials are included for each condition. It is also straightforward to design a severely underpowered study by including too few trials (here  $k<60$ ).

### fMRI: blocked design

An alternative fMRI paradigm is the blocked design, in which stimuli are presented for periods of several seconds, interleaved with periods of no stimulation. Typically, events are scheduled to coincide with the acquisition of functional

volumes (the repetition time, or TR). Blocked designs generally have greater power than event-related designs, because the stimulus timing is more closely aligned with the sluggish time constraints of haemodynamic activity, with the longer duration presentations (relative to event-related designs) allowing BOLD signals to sum over time (Boynton et al., 1996).

We reanalysed a data set comprising  $N=83$  participants, all of whom viewed a series of images of faces, objects, places and scrambled images as part of a functional localiser described by Flack et al. (2015). Stimuli were presented in blocks of 6 s, with a 9 s inter-block interval during which the display was blank. Within each block, 5 images were shown sequentially for 1000 ms each, with a 200 ms inter-stimulus interval. fMRI data were acquired with a TR of 3 s, so a complete cycle (one block plus inter-block interval) lasted for 15 s, or 5 TRs. Each participant completed  $k=35$  blocks. Functional data were high pass filtered, detrended and converted to percent signal change, and aligned to the MNI152 brain. The timeseries was then averaged across the V1 ROI shown in Figure 7a.

A timeseries for an example participant is shown in Figure 8a, and exhibits clear stimulus-driven modulations, with a period of 15 s matching that of the trial cycle. The BOLD response peaked 9 s after stimulus onset, as can be seen most clearly in Figure 8b, which averages the response across all 35 blocks for the example participant. The distributions of BOLD responses at each time point (relative to the start of a block) are shown in Figure 8c. Panels d-f of Figure 8 show comparable data for the population of  $N=83$  participants, displaying a similar pattern. In order to generate power contours for a range of effect sizes, we compared activity between sequential pairs of sample points. Effect sizes increased from  $d=0.26$  comparing 3 s and 0 s, to  $d=1.7$  comparing 6 s and 3 s. Power contours (see Figure 8g-j) approximately asymptoted for trial numbers above  $k=15$ . This pattern is somewhat different from the event-related fMRI results discussed previously (Figure 7), where adding more trials continued to increase power across the entire range. For the larger effects (Figure 8h-j), power was high even with the relatively small samples ( $N<20$ ) typical of many neuroimaging studies (Button et al., 2013). Of course looking for responses to visual stimuli in V1 is guaranteed to produce large effect sizes - most fMRI studies are designed to test subtler effects which will inevitably be smaller than in the examples here.

### MEG: evoked responses

The Cam-CAN data set also contains MEG responses ( $k=120$  trials) to the same visual stimuli as described in the section on event-related fMRI, recorded using a *VectorView* system (Elekta Neuromag, Helsinki). We filtered (0.01 -

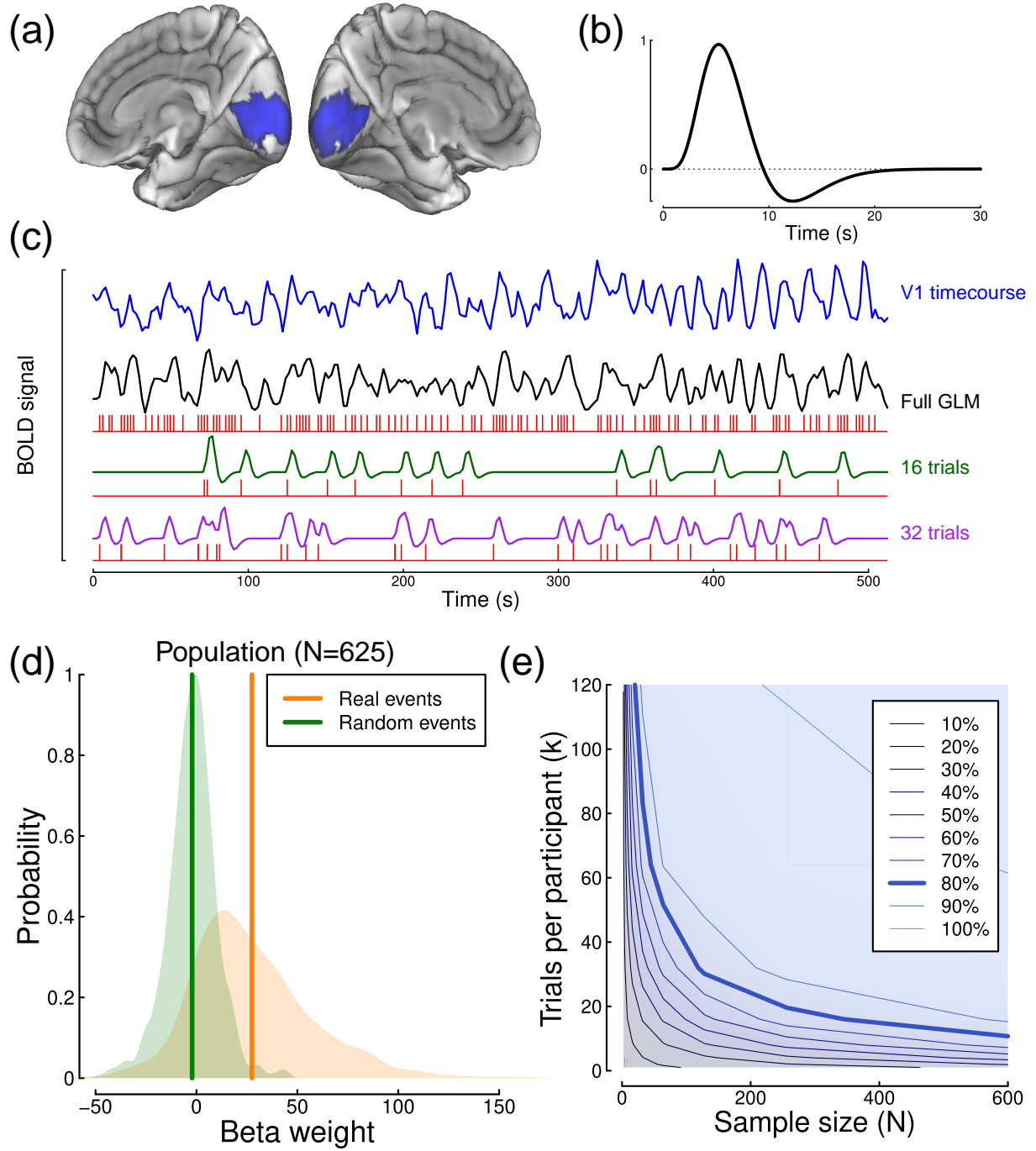


**Figure 7.** Summary of event-related fMRI analysis and results. Panel (a) shows the V1 region of interest on the medial surface of the standard (MNI152) brain, highlighted in blue. Panel (b) shows the canonical double gamma haemodynamic response function used in our general linear models. Panel (c) shows an example time-course from the V1 ROI for one participant (blue), and a general linear model constructed to predict this time-course (black) based on stimulus events (red). The green and purple traces show example GLM components with random subsets of trials. Panel (d) shows the population distributions of beta weights for the full GLM modelling all stimulus events (orange) or randomly simulated times (green). Panel (e) shows the power contour plot for these event-related fMRI data.

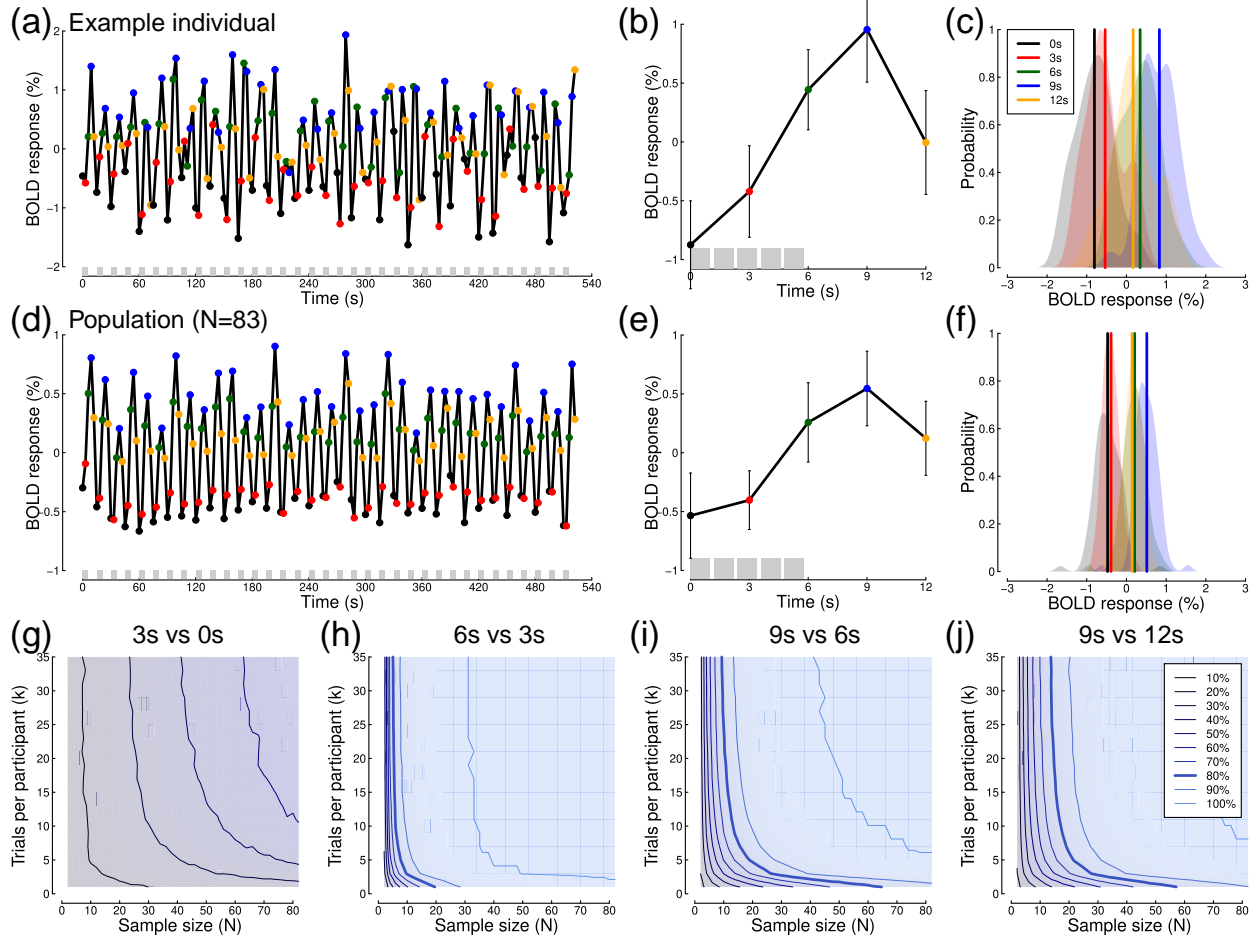


**Figure 8.** Summary of blocked design fMRI data. Panel (a) shows an fMRI timecourse for an example individual, averaged across the V1 ROI (see Figure 7a). Shaded grey regions at the foot of the panel indicate blocks when stimuli were presented. Panel (b) shows the data from panel (a) aligned to each block onset and averaged across all  $k=35$  blocks (with error bars showing  $\pm 1SD$ ). The grey shaded regions at the foot of the panel indicate the presentations of individual stimuli within a block. Panel (c) shows distributions of BOLD activity at each time point. Panels d-f mirror panels a-c but for the sample of  $N=83$  participants. Panels g-j show power contours for the fMRI data, comparing activity at successive time points.

30Hz bandpass) and epoched the data from each participant, and then conducted one-sample t-tests at a single sensor (see Figure 9a) comparing activity to zero. We selected three time points very soon after stimulus onset (50, 54 and 58  $ms$ ) to leverage the power of this large ( $N=637$ ) dataset, and to explore effects of a similar magnitude to those investigated in typical experiments, where small differences in responses to different stimuli or mental states might be compared.

Evoked responses showed an initial polarisation beginning around 50  $ms$ , followed by a larger peak of opposite polarity at 130  $ms$  (see Figure 9a). Effect sizes at the three time points increased from  $d = 0.17$  at 50  $ms$  to  $d = 0.51$  at 58  $ms$  when including all trials and participants. As for previous examples, the within-participant variance (Figure

9b) was clearly greater than the sample variance (Figure 9c). Power contours showed the familiar form (see Figure 9d-f), with power only reaching 80% for the 50  $ms$  time-point when the full data set was used. At later time points, iso-power contours show constant power can be maintained, for example when reducing the sample size from  $N=400$  to  $N=200$  by increasing the number of trials from  $k=20$  to  $k=60$  (at 54  $ms$ ).

## Discussion

We advocate a representation of statistical power as the joint function of sample size and number of trials; the power contour plot. Example power contours were generated using data sets from a number of widely used paradigms in

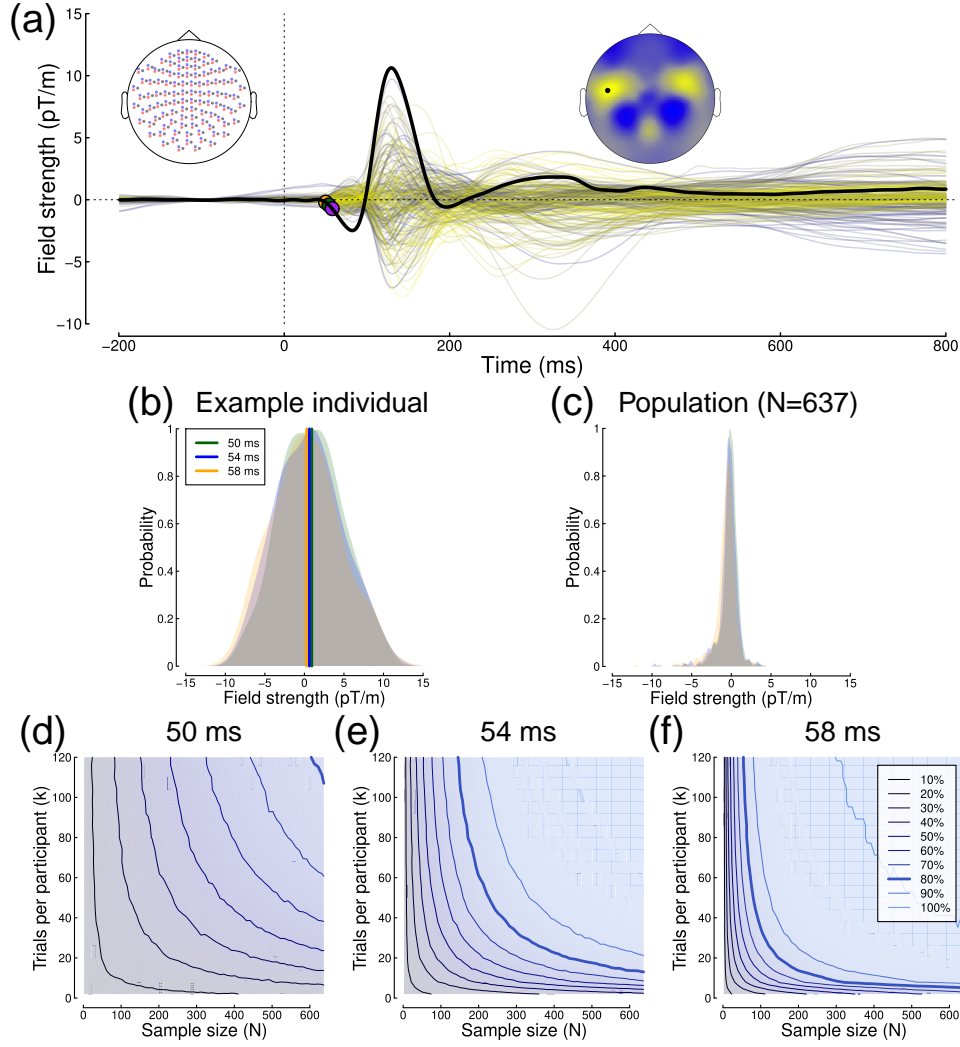


**Figure 9.** Summary of MEG results. Panel (a) shows a butterfly plot of evoked responses from 204 planar gradiometers, averaged across all participants ( $N=637$ ). The MEG montage is depicted in the upper left inset, where planar gradiometers of orthogonal orientations are indicated in blue and red, and magnetometer locations are shown in grey. The upper right inset shows the distribution of field strengths across a subset of 102 gradiometers with consistent orientation at 130 ms (the peak of the black curve), and the black dot indicates the location of the sensor used for the analysis. Coloured points highlighted on the black curve indicate time points used for power analysis. Panel (b) shows distributions of field strengths at each of the three target time points for an individual participant. Panel (c) shows the same but for the sample population of  $N=637$  participants. Panels (d-f) show power contours for different time-points.

experimental psychology and human neuroscience, covering a range of different sample sizes and trial numbers (summarised in Figure 10a). In most cases, iso-power contours revealed situations where statistical power could be maintained with fewer participants, provided that each participant completed a larger number of trials. For some paradigms, power reached asymptote at a particular number of trials, beyond which further testing conferred no benefit. In other paradigms, particularly those where the dependent variable

was derived by some form of model fit, power continued to improve with repeated testing, beyond the range that could be assessed with our data sets.

In Table 1, we summarise the relevant variables from each paradigm, including the mean effect, and within- and between-participant and sample standard deviations. Our expectation is that these values will be useful as a guide when planning future studies, as representative values for generating power contours. We pro-

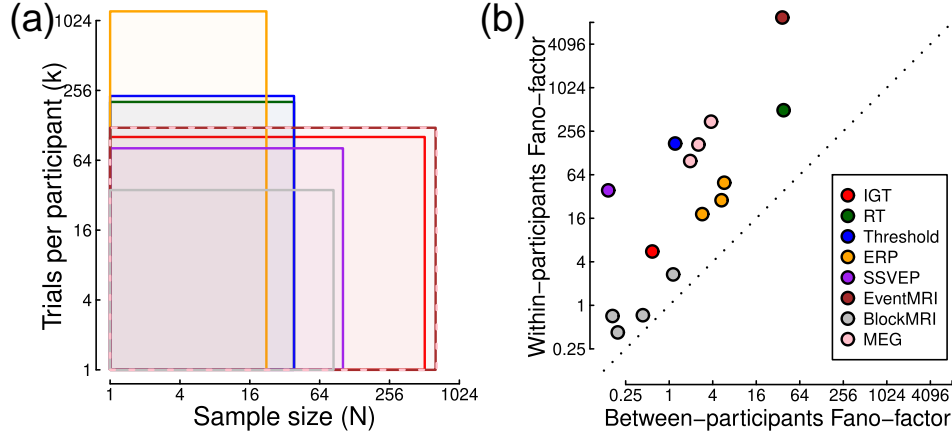


*Figure 10.* Summary of sample sizes, trial numbers and Fano-factors across experimental paradigms. Each rectangle in (a) covers the range of sample sizes and trial numbers for one of the studies analysed here, with colours defined in the legend in panel (b). Panel (b) plots Fano-factors (variance divided by the mean) derived from the within- and between-participants standard deviations given in Table 1. Note the log-scaled axes for both panels.

vide a web interface for simulating power contours (<https://shiny.york.ac.uk/powercontours/>), and all analysis scripts are available on the project OSF repository (<https://osf.io/ebhmk/>). For several paradigms, including sensory thresholds, SSVEPs, and event-related fMRI, estimates of within-participant standard deviations were not directly available because the process by which trials were combined did not generate one. In these cases, we simulated power contour surfaces for a range of candidate standard deviations, with the other parameters (mean and between-participant SD) fixed. We calculated the root mean squared error between each of these simulated surfaces and the empirically derived surfaces plotted throughout the manuscript. The estimated value is the within-participant standard deviation that produced the best fit.

We calculated the between participant standard deviation ( $\sigma_b$ ) by rearranging equation 1 to give:

$$\sigma_b = \sqrt{\sigma_s^2 - \frac{\sigma_w^2}{k}}. \quad (2)$$

In most cases the sample and between-participant standard deviations were similar, owing to the large number of trials conducted in the experiments analysed here. However this is unlikely to be the case for typical studies. For the SSVEP and event-related fMRI data sets, equation 2 returned an imaginary number because the estimated within-participant SD was very large. Here we assumed that  $\sigma_b = \sigma_s$  for the purposes of completing Table 1.

A further instructive analysis is to compare the within- and between-participant variances, as these provide insight

into the likely gains that can be obtained by conducting more trials on each participant. A situation in which the within-participant variance is very small compared to the between-participant variance will result in a power contour like that shown in Figure 1g, where repeated testing confers no benefit. Figure 10b plots the variances expressed as Fano-factors (variance scaled by the mean) to permit comparison across paradigms with widely differing units. It is clear that for all paradigms considered here, the within-participant variance is substantially above the between-participant variance (all points appear above the diagonal). This property is not a given, and we anticipate that there may be paradigms where within-participant variance is very low (owing to accurate measurement, or consistency of responses across multiple repetitions). We note that where multiple estimates were calculated for a single method (such as ERPs at different time points), the Fano-factors appear to cluster together, suggesting a consistent ratio of variances for a given paradigm. However this will require further investigation across multiple studies using a common methodology, and perhaps also across different laboratories and equipment (e.g. scanner models, sensor types etc).

Of course, we are far from the first to appreciate that repeated measurements can improve estimates of effect sizes. In the domain of psychometric research, the Spearman-Brown prophecy formula (Brown, 1910; Spearman, 1910) predicts how the reliability of a test (such as a personality test, or an IQ test) increases as more items are added. Other work has used cost functions to attempt to derive a single optimal experimental design, by assuming specific costs (usually in units of experimenter time) required for recruitment and testing of each participant (e.g. Cleary & Linn, 1969). In

Table 1

Summary of means, standard deviations and effect sizes for different paradigms. \*Estimated: to estimate a within-participant SD, we ran simulations to optimise the value of this parameter using the full power contour surface, see text for details.

| Paradigm                 | Mean effect    | Within-participant SD | Between-participant SD | Sample SD      | Effect size (d) |
|--------------------------|----------------|-----------------------|------------------------|----------------|-----------------|
| Iowa Gambling Task       | 0.04           | 0.47                  | 0.15                   | 0.16           | 0.24            |
| Reaction times           | 46 ms          | 150 ms                | 42 ms                  | 43 ms          | 1.1             |
| Sensory thresholds       | 6.6 dB         | 33.5 dB*              | 1.3 dB                 | 3.6 dB         | 1.8             |
| ERP 2 $\mu$ V            | 2 $\mu$ V      | 9.9 $\mu$ V           | 3.4 $\mu$ V            | 3.4 $\mu$ V    | 0.6             |
| ERP 4 $\mu$ V            | 4 $\mu$ V      | 10.6 $\mu$ V          | 4.6 $\mu$ V            | 4.6 $\mu$ V    | 0.9             |
| ERP 8 $\mu$ V            | 7.7 $\mu$ V    | 11.8 $\mu$ V          | 4.7 $\mu$ V            | 4.7 $\mu$ V    | 1.6             |
| SSVEP 8% vs 0%           | 0.25 $\mu$ V   | 3.1 $\mu$ V*          | 0.19 $\mu$ V           | 0.19 $\mu$ V   | 0.7             |
| Event-related fMRI       | $\beta = 28.6$ | $\beta = 515^*$       | $\beta = 32.2$         | $\beta = 32.2$ | 0.9             |
| Blocked fMRI 3 s vs 0 s  | 0.09%          | 0.49%                 | 0.32%                  | 0.33%          | 0.26            |
| Blocked fMRI 6 s vs 3 s  | 0.59%          | 0.50%                 | 0.34%                  | 0.35%          | 1.70            |
| Blocked fMRI 9 s vs 6 s  | 0.31%          | 0.47%                 | 0.23%                  | 0.24%          | 1.29            |
| Blocked fMRI 9 s vs 12 s | 0.37%          | 0.52%                 | 0.40%                  | 0.41%          | 0.91            |
| MEG 50 ms                | 0.20 pT/m      | 8.25 pT/m             | 0.87 pT/m              | 1.15 pT/m      | 0.17            |
| MEG 54 ms                | 0.42 pT/m      | 8.32 pT/m             | 1.03 pT/m              | 1.28 pT/m      | 0.32            |
| MEG 58 ms                | 0.72 pT/m      | 8.38 pT/m             | 1.18 pT/m              | 1.41 pT/m      | 0.51            |

principle these methods might be used to determine a point on the power contour that specifies a particular sample size and number of trials. We have avoided being prescriptive about this here, as different studies will have different constraints and priorities, and the advantage of visualising the entire power surface is that it permits the experimenter to trade off these two variables against each other without loss of power. However we have built functionality into the *Shiny* web application to estimate an optimal combination of sample size and number of trials, based on the additional constraint of a per-participant ‘recruitment cost’, expressed as a notional number of trials. The optimal point is calculated by determining the smallest value of  $N^*(k + \text{cost})$  that achieves 80% power. We advise caution in the use of this feature.

### Application to other statistical tests and approaches

Throughout all examples we have deliberately used a basic statistical test to determine power - the t-test. However the methods we develop here could very easily be extended to more advanced statistical methods, including Analysis of Variance (see Smith & Little, 2018, for a related example), correlation, regression and so on. For time-varying data using EEG and MEG (see Figures 5 & 9), it is commonplace to use cluster correction algorithms to control for multiple comparisons (e.g. Maris & Oostenveld, 2007). Informative power contours could in principle be constructed for significant clusters using either the number of trials (as here), or the number of time-points included within a cluster. Similar approaches might be applied to fMRI data, where the number of voxels included in a spatial cluster or a region of interest (ROI) will likely affect statistical power.

An alternative to null hypothesis significance testing is the Bayesian approach. Bayesian alternatives to t-tests often calculate a Bayes Factor (Rouder, Speckman, Sun, Morey, & Iverson, 2009) as a test statistic, which indicates the relative probabilities of experimental and null hypotheses. For a given experimental design, one could calculate ‘Bayes factor contours’ in an analogous manner to power contours, to estimate the number of trials and participants necessary to reach a specified level of evidence in support of one or other hypothesis. As Bayesian methods become more widespread, this may prove a useful alternative to traditional power analysis.

Another Bayesian-inspired method is to adaptively deploy data collection in the direction required to supply useful evidence to inform the outcome (posterior). An early example is the *Quest* algorithm (Watson & Pelli, 1983), used widely in psychophysics, which chooses the optimal stimulus level on each trial to provide the most information about the location of the threshold. Related methods have also been used to optimize data collection in fMRI experiments (Lorenz, Hampshire, & Leech, 2017). Typically such approaches operate at a per-participant level, and will result in efficient use of the time available. If the ultimate aim is to combine results statistically across participants, then power contours might still be used to optimise the number of trials, in a similar fashion to that shown here for the contrast detection data (Figure 4), which also involved an adaptive (staircase) procedure. On the other hand, if the algorithm is designed to continue until particular conditions are met, traditional power analysis based only on sample size may be more appropriate.

Most discussion of power analysis is focussed on stud-



ies which involve statistically demonstrating the presence of some effect. However an alternative approach common in perceptual and cognitive research is to explain and predict patterns of response across multiple conditions using a computational model. In this tradition, each participant can be considered an independent ‘replication’ of the phenomena under study (see e.g. Smith & Little, 2018), and the emphasis is on improving data quality through conducting many trials for each participant. Power contours might not be especially helpful under such circumstances, though knowledge of the within-participant standard deviation will inform decisions about how many trials to conduct.

## Conclusions

Here we present the rationale for incorporating the number of measurements (trials) into calculations of statistical power in experimental studies of psychology and human neuroscience. Power contour plots (which can be generated using an online tool) permit researchers to make informed choices about how many participants to test, and how long to test each one for, at the study design stage. To this end, we provide empirical estimates of both within- and between-participant standard deviations for a range of experimental paradigms that could be used as a guide when planning future studies. However, as with all *a priori* power calculations, the true effect sizes and variances will remain speculative until data have been collected.

## Acknowledgements

We are grateful to everyone involved in collection of the data sets reanalysed here, and particularly to those who made their data publicly available. We also thank Tom Hartley for helpful comments and for suggesting inclusion of the Iowa Gambling Task data set.

## References

- Baker, D. H., Lygo, F. A., Meese, T. S., & Georgeson, M. A. (2018). Binocular summation revisited: Beyond  $\sqrt{2}$ . *Psychol Bull*, 144(11), 1186–1199. doi: 10.1037/bul0000163
- Boynton, G. M., Engel, S. A., Glover, G. H., & Heeger, D. J. (1996). Linear systems analysis of functional magnetic resonance imaging in human V1. *J Neurosci*, 16(13), 4207–21.
- Brown, W. (1910). Some experimental results in the correlation of mental abilities. *British Journal of Psychology*, 3, 296–322.
- Button, K. S., Ioannidis, J. P. A., Mokrysz, C., Nosek, B. A., Flint, J., Robinson, E. S. J., & Munafò, M. R. (2013). Power failure: why small sample size undermines the reliability of neuroscience. *Nature Reviews Neuroscience*, 14(5), 365–376. doi: 10.1038/nrn3475
- Cleary, T. A., & Linn, R. L. (1969). Error of measurement and the power of a statistical test. *British Journal of Mathematical and Statistical Psychology*, 22(1), 49–55. doi: 10.1111/j.2044-8317.1969.tb00419.x
- Cohen, J. (1988). *Statistical power analysis for the behavioral sciences*. Lawrence Erlbaum Associates.
- Colquhoun, D. (2014). An investigation of the false discovery rate and the misinterpretation of p-values. *R Soc Open Sci*, 1(3), 140216. doi: 10.1098/rsos.140216
- Flack, T. R., Andrews, T. J., Hymers, M., Al-Mosaiwi, M., Marsden, S. P., Strachan, J. W., ... Young, A. W. (2015). Responses in the right posterior superior temporal sulcus show a feature-based response to facial expression. *Cortex*, 69, 14–23. doi: 10.1016/j.cortex.2015.03.002
- Grootswagers, T., Wardle, S. G., & Carlson, T. A. (2017). Decoding dynamic brain patterns from evoked responses: A tutorial on multivariate pattern analysis applied to time series neuroimaging data. *Journal of Cognitive Neuroscience*, 29(4), 677–697.
- Haynes, J.-D. (2015). A primer on pattern-based approaches to fMRI: Principles, pitfalls, and perspectives. *Neuron*, 87(2), 257–70. doi: 10.1016/j.neuron.2015.05.025
- Ioannidis, J. P. A. (2005, Aug). Why most published research findings are false. *PLoS Med*, 2(8), e124. doi: 10.1371/journal.pmed.0020124
- Ioannidis, J. P. A. (2008). Why most discovered true associations are inflated. *Epidemiology*, 19(5), 640–8. doi: 10.1097/EDE.0b013e31818131e7
- Jenkinson, M., Beckmann, C. F., Behrens, T. E. J., Woolrich, M. W., & Smith, S. M. (2012). FSL. *Neuroimage*, 62(2), 782–90. doi: 10.1016/j.neuroimage.2011.09.015
- Kanyongo, G. Y., Brook, G. P., Kyei-Blankson, L., & Gocmen, G. (2007). Reliability and Statistical Power: How Measurement Fallibility Affects Power and Required Sample Sizes for Several Parametric and Nonparametric Statistics. *Journal of Modern Applied Statistical Methods*, 6(1), 81–90. doi: 10.22237/jmasm/1177992480
- Linares, D., & López-Moliner, J. (2016). quickpsy: an R package to fit psychometric functions for multiple groups. *The R Journal*, 8(1), 122 - 131. doi: 10.32614/RJ-2016-008
- Lorenz, R., Hampshire, A., & Leech, R. (2017, 03). Neuroadaptive bayesian optimization and hypothesis testing. *Trends Cogn Sci*, 21(3), 155–167. doi: 10.1016/j.tics.2017.01.006
- Maris, E., & Oostenveld, R. (2007). Nonparametric statistical testing of EEG- and MEG-data. *Journal of Neu-*

- rosience Methods*, 164(1), 177–190. doi: 10.1016/j.jneumeth.2007.03.024
- Open Science Collaboration. (2015). Estimating the reproducibility of psychological science. *Science*, 349(6251), aac4716. doi: 10.1126/science.aac4716
- Phillips, G. W., & Jiang, T. (2016). Measurement error and equating error in power analysis. *Practical Assessment, Research & Evaluation*, 21(9), 12.
- Pirrone, A., Wen, W., Li, S., Baker, D. H., & Milne, E. (2018). Autistic traits in the neurotypical population do not predict increased response conservativeness in perceptual decision making. *Perception*, 47(10-11), 1081-1096. doi: 10.1177/0301006618802689
- Rouder, J. N., & Haaf, J. M. (2018). Power, Dominance, and Constraint: A Note on the Appeal of Different Design Traditions. *Advances in Methods and Practices in Psychological Science*, 1, 19-26.
- Rouder, J. N., Speckman, P. L., Sun, D., Morey, R. D., & Iverson, G. (2009). Bayesian t tests for accepting and rejecting the null hypothesis. *Psychonomic Bulletin & Review*, 16(2), 225–237. doi: 10.3758/pbr.16.2.225
- Schwarzkopf, D. S., & Rees, G. (2011). Pattern classification using functional magnetic resonance imaging. *Wiley Interdisciplinary Reviews: Cognitive Science*, 2(5), 568–579. doi: 10.1002/wcs.141
- Shafito, M. A., Tyler, L. K., Dixon, M., Taylor, J. R., Rowe, J. B., Cusack, R., ... Matthews, F. E. (2014). The Cambridge Centre for Ageing and Neuroscience (Cam-CAN) study protocol: a cross-sectional, lifespan, multidisciplinary examination of healthy cognitive ageing. *BMC Neurology*, 14(1). doi: 10.1186/s12883-014-0204-1
- Smith, P. L., & Little, D. R. (2018). Small is beautiful: In defense of the small-n design. *Psychon Bull Rev*, 25(6), 2083-2101. doi: 10.3758/s13423-018-1451-8
- Spearman, C. C. (1910). Correlation calculated from faulty data. *British Journal of Psychology*, 3, 271–295.
- Steingroever, H., Fridberg, D. J., Horstmann, A., Kjome, K. L., Kumari, V., Lane, S. D., ... Wagenmakers, E.-J. (2015). Data from 617 Healthy Participants Performing the Iowa Gambling Task: A “Many Labs” Collaboration. *Journal of Open Psychology Data*, 3. doi: 10.5334/jopd.ak
- Tabelow, K., & Polzehl, J. (2011). Statistical parametric maps for functional MRI experiments in R: the package fmri. *Journal of Statistical Software*, 44(11), 1 - 21. doi: 10.18637/jss.v044.i11
- Taylor, J. R., Williams, N., Cusack, R., Auer, T., Shafito, M. A., Dixon, M., ... Henson, R. N. (2017). The Cambridge Centre for Ageing and Neuroscience (Cam-CAN) data repository: Structural and functional MRI, MEG, and cognitive data from a cross-sectional adult lifespan sample. *NeuroImage*, 144, 262–269. doi: 10.1016/j.neuroimage.2015.09.018
- Vilidaite, G., Marsh, E., & Baker, D. H. (2019). Internal noise in contrast discrimination propagates forwards from early visual cortex. *NeuroImage*, under review.
- Vilidaite, G., Norcia, A. M., West, R. J. H., Elliott, C. J. H., Pei, F., Wade, A. R., & Baker, D. H. (2018). Autism sensory dysfunction in an evolutionarily conserved system. *Proceedings of the Royal Society B*, 285, 20182255. doi: 10.1098/rspb.2018.2255
- Wang, L., Mruczek, R. E. B., Arcaro, M. J., & Kastner, S. (2015). Probabilistic maps of visual topography in human cortex. *Cereb Cortex*, 25(10), 3911-31. doi: 10.1093/cercor/bhu277
- Watson, A. B., & Pelli, D. G. (1983). Quest: a bayesian adaptive psychometric method. *Percept Psychophys*, 33(2), 113-20.
- Williams, R. H., & Zimmerman, D. W. (1989). Statistical Power Analysis and Reliability of Measurement. *The Journal of General Psychology*, 116(4), 359–369. doi: 10.1080/00221309.1989.9921123